ACS Catalysis

Letter

pubs.acs.org/acscatalysis

Deconstructing Selectivity in the Gold-Promoted Cyclization of Alkynyl Benzothioamides to Six-Membered Mesoionic Carbene or Acyclic Carbene Complexes

Sai Vikrama Chaitanya Vummaleti,[†] Laura Falivene,[§] Albert Poater,[‡] and Luigi Cavallo*[,†]

[†]Kaust Catalysis Center, Physical Sciences and Engineering Division, King Abdullah University of Science and Technology, Thuwal 23955-6900, Saudi Arabia

[§]Dipartimento di Chimica e Biologia, Università di Salerno, Via Giovanni Paolo II, 84084 Fisciano, Italy

[‡]Institut de Química Computacional i Catàlisi and Departament de Química, Universitat de Girona, Campus Montilivi, 17071 Girona, Catalonia, Spain

Supporting Information

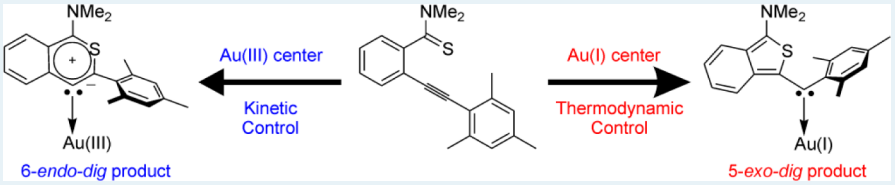

ABSTRACT: We demonstrate that the experimentally observed switch in selectivity from 5-exo-dig to 6-endo-dig cyclization of an alkynyl substrate, promoted by Au^{I} and Au^{III} complexes, is connected to a switch from thermodynamic to kinetic reaction control. The Au^{III} center pushes alkyne coordination toward a single Au−C(alkyne) σ-bond, conferring carbocationic character (and reactivity) to the distal alkyne C atom.

KEYWORDS: *gold catalysis, mesoionic carbene, density functional theory, thermodynamic and kinetic control, ab initio molecular dynamics*

Gold-promoted catalysis[1] has opened the route to a countless number of new organic transformations, including the clever synthesis of novel compounds, such as complexes **5A** and **6B** of Scheme 1.[2] The former is the first example of a diarylcarbene−gold complex, and the latter is the first reported example of a gold complex featuring a non-nitrogen-containing six-membered mesoionic carbene.[3] The elegance and power of gold-promoted reactivity allowed achieving the synthesis of these two novel complexes starting from the same alkynyl benzothioamide precursor, **1** of Scheme 1, by simply using AuCl, **A**; or $AuCl_3$, **B**.

Scheme 1. Selective Cyclization of 1 Induced by Au^{I} and Au^{III} Species

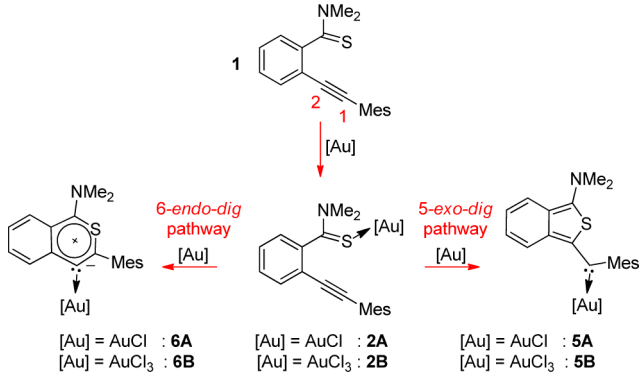

In addition to the remarkable synthesis of novel compounds, these results indicated a change in the oxidation state of the metal center as a route to switch cyclization from the more common 5-exo-dig route,[4,5] leading in this case to **5A**; to the less frequently encountered 6-endo-dig route,[4,6] leading in this case to **6B**. Understanding the reasons for this behavior can offer conceptual tools to think of new applications in the field. With this aim, we offer here a theoretical rationalization[7] of the experimental results.[8] Interestingly, our results indicate that the selective 5-exo-dig cyclization in the presence of Au^{I} is thermodynamically controlled, whereas the preference for 6-endo-dig in the presence of Au^{III} is kinetically controlled.

Cyclization of **2** promoted by (tht)AuCl (tht = tetrahydrothiofurane) starts with displacement of tht by the thioamide functionality of **1**, leading to the S-coordinated complex **2A**, also characterized experimentally. Displacement of tht is favored by only 0.3 kcal/mol (see Figure 1), which is nicely consistent with the experimental yield of 65% achieved in the synthesis of **2A** from equimolar amounts of (tht)AuCl and **1**.[2] We consider this result as a validation of the computational

Received: February 6, 2014
Revised: March 15, 2014
Published: March 17, 2014

   dx.doi.org/10.1021/cs5001575 | ACS Catal. 2014, 4, 1287−1291

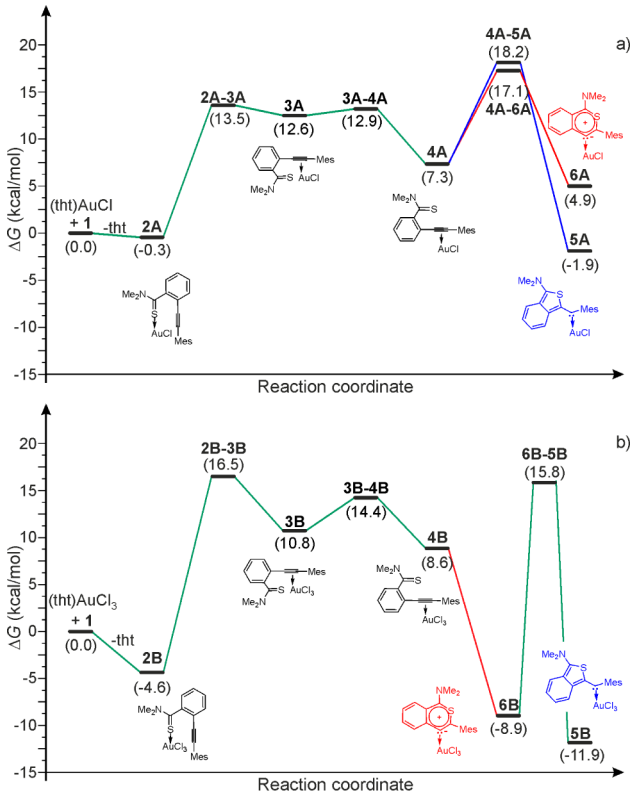

Figure 1. Free energy surface of (a) AuCl- and (b) $AuCl_3$-promoted transformation of **1**.

recipe used in this work. Because direct cyclization from the S-coordinated intermediates can be excluded,[6a] we started with the conformational rearrangement of **2A** leading to **4A**, with the alkyne functionality coordinated to the Au center, and the thioamide functionality above the Au center, ready to attack the alkyne. Intermediate **4A** lies 7.6 kcal/mol above **2A**, and it is easily reached through a two-step process consisting of =S displacement by the alkyne; through transition state **2A**−**3A**, lying only 13.8 kcal/mol above **2A**, followed by a rotation of the thioamide-substituted aryl ring; through transition state **3A**−**4A**, lying only 13.2 kcal/mol above **2A**; to bring the thioamide functionality in a position ready for nucleophilic attack to the alkyne. Cyclization of **4A** through the nucleophilic attack of the S atom to the C2 atom of the activated alkyne functionality leads to the observed 5-exo-dig product **5A**, and attack on the C1 atom leads to the nonreported 6-endo-dig product **6A**.

According to calculations, both cyclizations can occur easily, with barriers around 10 kcal/mol for the last step starting from **4A**, and an overall barrier of ∼20 kcal/mol from **2A**. However, of relevance here is that transition state **4A**−**6A** is 1.1 kcal/mol lower in energy than transition state **4A**−**5A**, which indicates that formation of the nonreported product **6A** should be kinetically favored, although this preference is small.[9] As for the thermodynamics of the reaction, the nonreported product **6A** is predicted to be 5.2 kcal/mol above intermediate **2A**, and the observed product **5A** is predicted to lie 1.6 kcal/mol below **2A**. Overall, the energy profile shown in Figure 1 offers a clear explanation for the preferential formation of the observed product **5A**. In fact, 6-endo-dig cyclization can even be kinetically slightly favored over 5-exo-dig cyclization, but the **6**-endo-dig product **6A** is unstable so that it reversibly rearranges to **4A**, which either returns to the thioamide-coordinated species **2A** or collapses into the thermodynamically favored product **5A**. The low barrier for the reverse reaction regenerating **4A** from **6A**, only 12.2 kcal/mol, ensures the reversibility of the 6-endo-dig cyclization.

We now turn to describing cyclization of **1** promoted by Au^{III}, initially considered as $(tht)AuCl_3$. Displacement of tht by the thioamide functionality of **1**, leading to the S-coordinated intermediate **2B**, is favored by 4.6 kcal/mol. Two-step rearrangement of **2B** leads to **4B**, with the alkyne functionality coordinated to the Au center and the substrate ready to undergo cyclization. Intermediate **4B** lies 13.2 kcal/mol above **2B**, and it is reached through transition states **2B**−**3B** and **3B**−**4B**, lying 21.1 and 19.0 kcal/mol, respectively, above **2B**.

Cyclization of **4B** through a nucleophilic attack of the S atom to the C2 atom of the activated alkyne functionality leads to the nonreported 5-exo-dig product **5B**, whereas attack on the C1 atom leads to the observed 6-endo-dig product **6B**. Although a transition state corresponding to formation of **5B** could be located easily, at 7.2 kcal/mol above **4B**, it was impossible to locate a transition state corresponding to formation of **6B**.[10] This suggests that **4B** is a metastable intermediate of scarce kinetic relevance that directly collapses into **6B**. The barrierless 6-endo-dig cyclization from intermediate **4B**, together with a sizable barrier for the 5-exo-dig cyclization, suggests a bifurcation of the potential energy surface after **4B**.[11] To have a better understanding of this point, we investigate the evolution of transition state **3B**−**4B** from a dynamic point of view.[12] To this end, we evolved molecular dynamics trajectories backward and forward in time from **3B**−**4B**, until we harvested 25 reactive trajectories (a trajectory is considered reactive if it connects reactants and products, see the SI for further details). The time evolution of the S−C1 and S−C2 distances along the 25 trajectories starting from **3B**−**4B** is shown in Figure 2a.

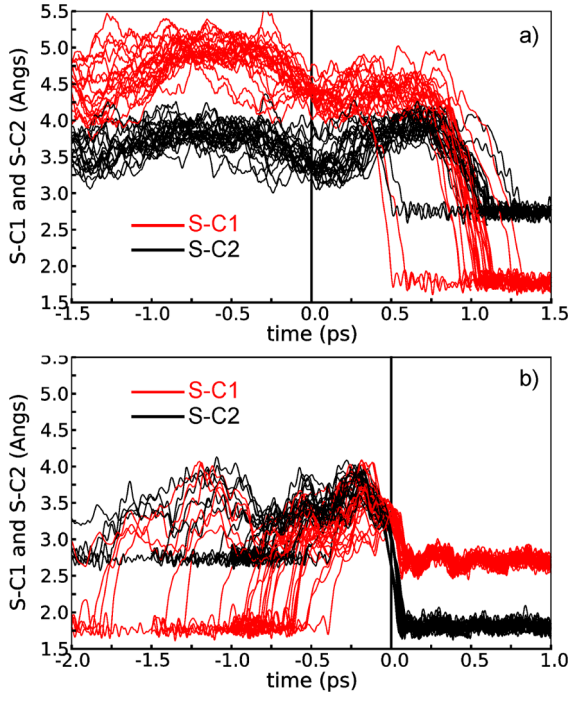

Figure 2. Time evolution of the S−C1 and S−C2 distances along 25 reactive trajectories started from transition states **3B**−**4B** (a) and **6B**−**5B** (b). Transition states **3B**−**4B** and **6B**−**5B**, are located at t = 0.

dx.doi.org/10.1021/cs5001575 | ACS Catal. 2014, 4, 1287−1291

Inspection of the Figure clearly shows that in all the 25 trajectories examined, the S−C1 distance collapses to values around 1.8 Å moving forward in time from **3B**−**4B**, indicative of 6-endo cyclization, within 1.5 ps. This confirms that transition state **3B**−**4B** evolves effortlessly to **6B**, passing quickly over the flat valley corresponding to the intermediate **4B**. On the other side, moving **3B**−**4B** backward in time precipitates the system back to the alkyne-coordinated intermediate **3B**, with rather large S−C1 and S−C2 distances.

To have an overall view of the energy surface and to better characterize the transition state corresponding to 5-exo cyclization, we harvested 25 reactive dynamic trajectories starting from the transition state for 5-exo-dig cyclization (see Figure 2b). The time evolution of the S−C1 and S−C2 distances indicates that in the forward trajectories, the S−C2 distance that collapses to values around 1.8 Å, indicative of the expected 5-exo cyclization. Interestingly, all the backward trajectories do not stop at intermediate **4B**, but after some longer time precipitate into the 6-endo-dig product **6B**, as indicated by the S−C1 distance collapsing to values around 1.8 Å. This indicates that the located transition state connects **6B** and **5B**, and thus, it is better indicated as transition state **6B**−**5B**.[13]

The overall potential energy surface derived from combining the reactive trajectories (see Figure 3) shows the rather flat

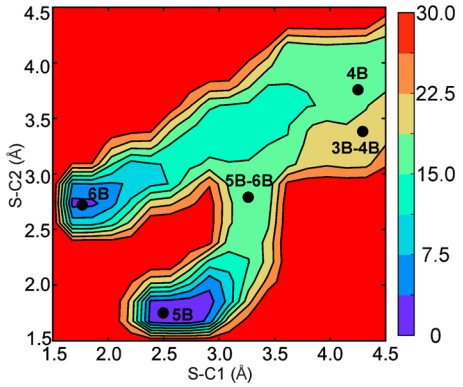

Figure 3. Potential energy profile of **3B**−**4B** as a function of the S−C1 and S−C2 distances from the 25 reactive trajectories reported in Figure 2. Isocontours separation is of 5 kcal/mol.

valley, with no energy barrier, connecting almost straightforwardly transition state **3B**−**4B** to the 6-endo-dig product **6B**. This broad energy plateau is also consistent with the plots of Figure 2, both showing that the system somehow oscillates before collapsing into **6B**. Differently, the extremely fast collapse of transition state **6B**−**5B** into the 5-exo-dig product **5B** of Figure 2b is consistent with the narrow and steep groove connecting **6B**−**5B** to **5B**.

The above molecular dynamics analysis allows one to properly build the energy profile of Figure 1b, with a two intermediate and no transition state profile[11] connecting **4B** to **6B** and with the transition state for 5-exo-dig cyclization connecting the two products, **5B** and **6B**. Focusing on the thermodynamics of the reaction, the static calculations reported in Figure 1b indicate that the nonreported product **5B** is predicted to be 7.3 kcal/mol below intermediate **2B**, whereas the observed product **6B** is predicted to lie 4.3 kcal/mol below **2B** and 3.0 kcal/mol above the product **5B**. In other words, also in the case of cyclization promoted by $AuCl_3$, the 6-endo-dig pathway is favored kinetically but unfavored thermodynamically. However, there is one remarkable difference between the two energy profiles: with AuCl, the two cyclization products are not directly connected and are reached from the common open cycle intermediate **4A**, whereas with $AuCl_3$, the five-membered product **5B** is formed from isomerization of the six-membered product **6B**. The energy barrier for the reaction converting **6B** into **5B** (through transition state **6B**−**5B**) amounts to 24.7 kcal/mol, which is at the limit of what can be considered feasible at room temperature. To sum up, our results indicate that cyclization in the presence of Au^{I} is thermodynamically controlled, but for Au^{III}, it is kinetically controlled.

Moving to the difference in the energy barrier for cyclization from the alkyne coordinated complexes **4A** and **4B**, this can be rationalized considering that the more electrophilic $AuCl_3$ fragment[14] activates more the alkyne functionality, as evidenced by the geometries reported in Figure 4. The binding of the

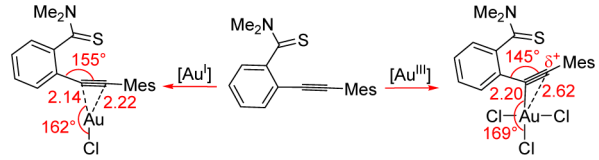

Figure 4. Effect of the Au oxidation state on the Au−alkyne bonding. Au−C1 and Au−C2 distances in Å.

alkyne moiety in **4A** is more symmetric, with the Au−C1 distance only 0.08 Å longer than the Au−C2 distance, whereas alkyne coordination in **4B** is clearly more asymmetric, with the Au−C1 distance 0.42 Å longer. Further, the C1−C(mesityl) distance is 1.44 Å in **4A**, and it is shortened to 1.40 Å in **4B**. Finally, natural population analysis, NPA,[15] indicates a greater polarization of the alkyne bond in **4B**, with localization of a +0.26 NPA charge on the C1 atom, compared with NPA charges of −0.10*e* and +0.03*e* on the C2 and C1 atoms of **4A** (see Figure 5a,b).

All together, this is a clear indication that the Au−alkyne bond has a strong π character in **4A**, and the Au^{III} center shifts

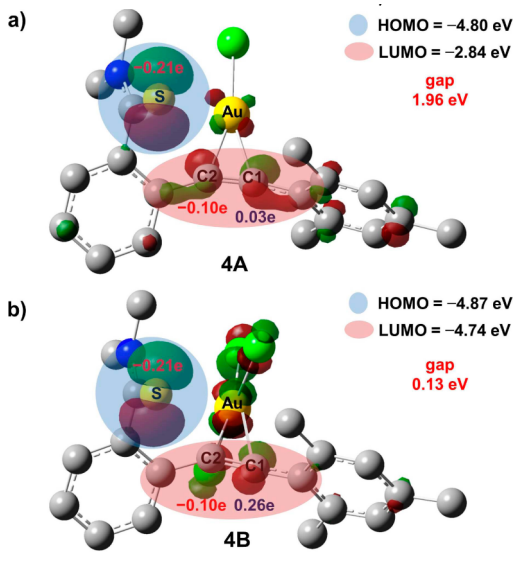

Figure 5. NPA charges and frontier molecular orbitals of intermediates **4A** and **4B**, parts a and b. H atoms have been omitted for clarity. MOs surface plotted at 0.08 au.

dx.doi.org/10.1021/cs5001575 | *ACS Catal.* 2014, 4, 1287−1291

the Au−alkyne interaction toward σ-bonding in **4B**, with the C1 atom assuming a carbocationic character, as shown in Figure 5. This is confirmed by the Mayer bond order of the Au−C1 and Au−C2 bonds, which are 0.50 and 0.56 in **4A**, whereas in **4B**, they are 0.19 and 0.52.

The rather similar NPA charge on the C2 atom in **4A** and **4B** is consistent with rather similar barriers for 5-exo-dig cyclization in the Au^{I} and Au^{III} systems, but the carbocationic character of the C1 atom of **4B** explains the barrierless 6-endo-dig cyclization in the Au^{III} system. Analysis of the frontier molecular orbitals indicates that the HOMO corresponds to a lone pair in a p orbital of the S atom in both **4A** and **4B**, but the LUMO is essentially a π^* orbital located on the alkyne functionality, equally distributed on C2 and C1 atoms (11% and 16%, respectively) in **4A**. It is essentially an empty p orbital located only on the C1 atom in **4B**, 15%. Further, the HOMO−LUMO gap is 1.96 eV in **4A**, but it reduces to 0.13 eV only in **4B**, consistent with the barrierless cyclization from **4B**.

Having rationalized the behavior of the systems proposed in the literature, we explored the effect of manipulating the substrate electronics to induce 6-endo-dig cyclization with Au^{I}.[16] To this end, we calculated the relative stability of the cyclization products **5A** and **6A** relative to the starting species **2A** for a series of substrates, with the aim of finding one that could lead to a six-membered mesoionic carbene with a Au^{I} center. Although a detailed discussion of these hypothetical substrates **1a**−**1j** is reported in the SI, we only note here that **1i** could, indeed, allow this synthesis, since 6-endo-dig cyclization is favored kinetically, and the corresponding six-membered mesoionic carbene product is thermodynamically more stable than the starting thioamide-coordinated species.

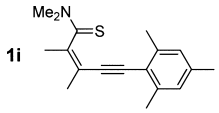

In summary, we have demonstrated that the switch in selectivity observed in the cyclization of alkynes benzothioamide substrates is due to a switch in the bonding between the Au center and the substrate. Specifically, the more electron-rich Au^{I} center favors a classic symmetric π-binding of the alkyne, whereas the Au^{III} center pushes the alkyne toward σ-bonding, resulting in the C-alkyne atom away from the Au center assuming a carbocationic character. This asymmetric bonding of the alkyne induces nonstandard reactivity, including bifurcation events.[11] We believe that this understanding can be used to think of novel reactivity, especially in the emerging field of Au^{III} catalysis.[6d,16,17]

■ ASSOCIATED CONTENT

Supporting Information

Computational details, Cartesian coordinates, PES scan around **4B**, energy decomposition analysis of **3A** and **4A**, dynamic analysis of transition state **3A**−**4A**, Au^{I}-promoted cyclization of hypothetical substrates. Movies of representative MD simulations. This material is available free of charge via the Internet at http://pubs.acs.org.

■ AUTHOR INFORMATION

Corresponding Author

*E-mail: luigi.cavallo@kaust.edu.sa.

Notes

The authors declare no competing financial interest.

■ REFERENCES

(1) For reviews on gold-catalyzed chemistry, see: (a) Hashmi, A. S. K. *Chem. Rev.* **2007**, *107*, 3180−3211. (b) Füstner, A.; Davies, P. W. *Angew. Chem., Int. Ed.* **2007**, *46*, 3410−34349. (c) Gorin, D. J.; Toste, F. D. *Nature* **2007**, *446*, 395−403. (d) Li, Z.; Brouwer, C.; He, C. *Chem. Rev.* **2008**, *108*, 3239−3265. (e) Arcadi, A. *Chem. Rev.* **2008**, *108*, 3266−3325. (f) Jiménez-Nunez, E.; Echavarren, A. M. *Chem. Rev.* **2008**, *108*, 3326−3350. (g) Gorin, D. J.; Sherry, B. D.; Toste, F. D. *Chem. Rev.* **2008**, *108*, 3351−3378. (h) Patil, N. T.; Yamamoto, Y. *Chem. Rev.* **2008**, *108*, 3395−3442. (i) Diez-González, S.; Nolan, S. P. *Acc. Chem. Res.* **2008**, *41*, 349−358. (j) Fürstner, A. *Chem. Soc. Rev.* **2009**, *38*, 3208−3221. (k) Rudolph, M.; Hashmi, A. S. K. *Chem. Soc. Rev.* **2012**, *41*, 2448−2462.

(2) Ung, G.; Soleilhavoup, M.; Bertrand, G. *Angew. Chem., Int. Ed.* **2013**, *51*, 758−761.

(3) For reviews on mesoionic carbene chemistry, see: (a) Schuster, O.; Yang, L.; Raubenheimer, H. G.; Albrecht, M. *Chem. Rev.* **2009**, *109*, 3445−3478. (b) Albrecht, M. *Chem. Commun.* **2008**, 3601−3610. (c) Arnold, P. L.; Pearson, S. *Coord. Chem. Rev.* **2007**, *251*, 596−609. (d) Melaimi, M.; Soleilhavoup, M.; Bertrand, G. *Angew. Chem., Int. Ed.* **2010**, *49*, 8810−8849. (e) Martin, D.; Melaimi, M.; Soleilhavoup, M.; Bertrand, G. *Organometallics* **2011**, *30*, 5304−5313.

(4) (a) Baldwin, J. E. *J. Chem. Soc, Chem. Comm.* **1976**, *18*, 734−736. (b) Alabugin, I.; Gilmore, K.; Manoharan, M. *J. Am. Chem. Soc.* **2011**, *133*, 12608−12623.

(5) See, for examples: (a) Hashmi, A. S. K.; Schuster, A. M.; Rominger, F. *Angew. Chem.* **2009**, *121*, 8396; *Angew. Chem., Int. Ed.* **2009**, *48*, 8247−8249. (b) Egorova, O. A.; Seo, H.; Kim, Y.; Moon, D.; Rhee, Y. M.; Ahn, K. H. *Angew. Chem.* **2011**, *123*, 11648−11652; *Angew. Chem., Int. Ed.* **2011**, *50*, 11446−11450.

(6) See, for examples: (a) Nevado, C.; Cárdenas, D. J.; Echavarren, A. M. *Chem.—Eur. J.* **2003**, *9*, 2627−2635. (b) Genin, E.; Toullec, P. Y.; Antoniotti, S.; Brancour, C.; Genêt, J.-P.; Michelet, V. *J. Am. Chem. Soc.* **2006**, *128*, 3112−3113. (c) Ritter, S.; Horino, Y.; Lex, J.; Schmalz, H.-G. *Synlett* **2006**, 3309−3313. (d) Hashmi, A. S. K.; Schuster, A. M.; Gaillard, S.; Cavallo, L.; Poater, A.; Nolan, S. P. *Organometallics* **2011**, *30*, 6328−6337. (e) Barabé, F.; Levesque, P.; Korobkov, I.; Barriault, L. *Org. Lett.* **2011**, *13*, 5580−5583.

(7) For theoretical papers on gold chemistry, see: (a) Kovács, G.; Lledós, A.; Ujaque, G. *J. Am. Chem. Soc.* **2008**, *130*, 853−864. (b) Cuenca, A. B.; Montserrat, S.; Hossain, K. M.; Mancha, G.; Lledós, A.; Medio-Simón, M.; Ujaque, G.; Asensio, G. *Org. Lett.* **2009**, *11*, 4906−4909. (c) Alonso, I.; Trillo, B.; López, F.; Montserrat, S.; Ujaque, G.; Castedo, L.; Lledós, A.; Mascareiñas, J. L. *J. Am. Chem. Soc.* **2009**, *131*, 13020−13030. (d) Pérez, A. G.; López, C. S.; Marco-Contelles, J.; Faza, O. N.; Soriano, E.; de Lera, A. R. *Org. Chem* **2009**, *74*, 2982−2991. (e) Liu, L.; Malhotra, D.; Paton, R. S.; Houk, K. N.; Hammond, G. B. *Angew. Chem., Int. Ed.* **2010**, *49*, 9132−9135. (f) Müller, R. S.; Gaillard, S.; Poater, A.; Cavallo, L.; Slawin, A. M. Z.; Nolan, S. P. *Chem.—Eur. J.* **2011**, *17*, 1238−1246. (g) Nun, P.; Dupuy, S.; Gaillard, S.; Poater, A.; Cavallo, L.; Nolan, S. P. *Catal. Sci. Technol.* **2011**, *1*, 58−61. (h) Soriano, E.; Marco-Contelles, J. *J. Org. Chem.* **2012**, *77*, 6231−6238. (i) Fang, R.; Yang, L. *Organometallics* **2012**, *31*, 3043−3055. (j) Muuronen, M.; Perea-Buceta, J. E.; Nieger, M.; Patzschke, M.; Helaja, J. *Organometallics* **2012**, *31*, 4320−4330.

(8) The G09 package was used to optimize geometries at the BP86 level with the SVP/SDD basis set. The reported energies correspond to M06 energies in solvent (THF) with the TZVP basis set. See the SI.

(9) To test the impact of the functional and basis set on the energy difference between transition states **4A**−**5A** and **4A**−**6A**, we located both transition states at the M06/TZVP level. At this level, transition state **4A**−**6A** is favoured by 2.0 kcal/mol in the gas phase, replicating the BP86/SVP preference in the gas phase, 2.1 kcal/mol.

(10) A PES scan in the range 4.3−1.8 Å for the forming S−C1 bond indicated a substantially flat PES at the beginning, which allows locating intermediate **4B**, followed by a downhill energy profile; see Figure S2 in the SI. We tested this result at the M06/TZVP level, but also in this case we were not able to locate transition state **4B**−**6B**, with efforts collapsing into **4B** or **6B**.

(11) (a) Rehbein, J.; Carpenter, B. K. *Phys. Chem. Chem. Phys.* **2011**, *13*, 20906−20922. (b) Noey, E. L.; Wang, X.; Houk, K. N. *J. Org. Chem.* **2011**, *76*, 3477−3483. (c) Garayalde, D.; Gomez-Bengoa, E.; Huang, X.; Goeke, A.; Nevado, C. *J. Am. Chem. Soc.* **2010**, *132*, 4720−4730. (d) Wang, Z. J.; Benitez, D.; Tkatchouk, E.; Goddard, W. A., III; Toste, D. F. *J. Am. Chem. Soc.* **2010**, *132*, 13064−13071. (e) Noey, E. L.; Luo, Y.; Zhang, L.; Houk, K. N. *J. Am. Chem. Soc.* **2012**, *134*, 1078−1084. (f) Hong, Y. J.; Tantillo, D. J. *Nat. Chem.* **2009**, *1*, 384−389. (g) Hong, Y. J.; Tantillo, D. J. *Nat. Chem.* **2014**, *6*, 104−111.

(12) MD simulations were run with the CP2K package at the PBE level using the DZVP-GTH basis set, with a 300 Ry cutoff. See the SI.

(13) Similar dynamic analysis was performed from transition state **3A**−**4A**. In all the cases, the forward evolution stopped at intermediate **4A**. Further analysis is reported in the SI.

(14) Further analysis is reported in the SI.

(15) (a) Reed, A. E.; Weinhold, F. *J. Chem. Phys.* **1983**, *78*, 4066−4073. (b) Reed, A. E.; Curtiss, L. A.; Weinhold, F. *Chem. Rev.* **1988**, *88*, 899−926.

(16) (a) Gupta, S.; Koley, D.; Ravikumar, K.; Kundu, B. *J. Org. Chem.* **2013**, *78*, 8624−8633. (b) Oppedisano, A.; Prandi, C.; Venturello, P.; Deagostino, A.; Goti, G.; Scarpi, D.; Occhiato, E. G. *J. Org. Chem.* **2013**, *78*, 11007−11016.

(17) (a) Peng, Y.; Cui, L.; Zhang, G.; Zhang, L. *J. Am. Chem. Soc.* **2009**, *131*, 5062−5063. (b) Egorova, O. A.; Seo, H.; Kim, Y.; Moon, D.; Rhee, Y. M.; Ahn, K. H. *Angew. Chem., Int. Ed.* **2011**, *50*, 11446−11450. (c) Muuronen, M.; Perea-Buceta, J. E.; Nieger, M.; Patzschke, M.; Helaja, J. *Organometallics* **2012**, *31*, 4320−4330. (d) Hashmi, A. S. K. *Angew. Chem., Int. Ed.* **2012**, *51*, 12935−12936. (e) Wolf, W. J.; Winston, M. S.; Toste, D. F. *Nat. Chem.* **2014**, *6*, 159−164.